Structural Optimization 15, 81–91 © Springer-Verlag 1998

Adaptive topology optimization of elastoplastic structures

K. Maute, S. Schwarz and E. Ramm

Institute of Structural Mechanics, University of Stuttgart, Pfaffenwaldring 7, D-70550 Stuttgart, Germany

Abstract Material topology optimization is applied to determine the basic layout of a structure. The nonlinear structural response, e.g. buckling or plasticity, must be considered in order to generate a reliable design by structural optimization. In the present paper adaptive material topology optimization is extended to elastoplasticity. The objective of the design problem is to maximize the structural ductility which is defined by the integral of the strain energy over a given range of a prescribed displacement. The mass in the design space is prescribed. The design variables are the densities of the finite elements. The optimization problem is solved by a gradient based OC algorithm. An elastoplastic von Mises material with linear, isotropic work-hardening/softening for small strains is used. A geometrically adaptive optimization procedure is applied in order to avoid artificial stress singularities and to increase the numerical efficiency of the optimization process. The geometric parametrization of the design model is adapted during the optimization process. Elastoplastic structural analysis is outlined. An efficient algorithm is introduced to determine the gradient of the ductility with respect to the densities of the finite elements. The overall optimization procedure is presented and verified with design problems for plane stress conditions.

1 Introduction

During the last years numerous methods for topology optimization of discrete and continuous structures have been introduced and applied to a broad range of design problems. An overview can be found in the proceedings edited by Bendsøe and Mota Soares (1991), the review paper by Rozvany *et al.* (1995) and the book by Bendsøe (1995). The layout problem is transferred into a material distribution problem. The body of a structure is defined, whether or not there is material at a point $\mathbf{x}$ in the design space Ω,

$$\mathbf{X} : \chi(\mathbf{x}) = \begin{cases} 0 \rightarrow \text{no material} \\ 1 \rightarrow \text{material} \end{cases} \quad \chi \in L_\infty(\Omega)\,,\ \mathbf{x} \in I\!R^3(\Omega)\,. \tag{1}$$

The indicator function $\chi(\mathbf{x})$ is equal to "0" if there is no material or equal to "1" if there is material in point $\mathbf{x}$. Only one homogeneous, isotropic material in the design space is assumed. In a discretized formulation the search for the optimum material distribution in the design space corresponds to a combinatorial problem which is very costly to solve. The arbitrarily discontinuous description of material distribution leads to a highly nonconvex variational problem which can be overcome by introducing porous materials (Kohn and Strang 1986). The integer problem is transferred into a continuous problem. The discrete valued parameter function χ becomes a continuous distribution of a new parameter $\overline{\chi} : 0 < \overline{\chi} < 1$ which means the density of the porous material. In a physically orientated approach the macroscopic material properties are derived from the microscopic structure of the porous material by homogenization. The optimization variables describe the geometry of the microstructure. In the SIMP approach (Solid Isotropic Microstructure with Penalty for intermediate densities) the optimization variables are macroscopic material properties such as density or Young's modulus (Rozvany and Zhou 1990; Rozvany *et al.* 1992; Mlejnek 1993; Maute and Ramm 1995a).

The material distribution $\overline{\chi}$ is piecewise approximated by $\overline{\chi}_i$ in order to solve numerically the relaxed optimization problem. This discretization is usually identical to the finite element discretization, which is used for structural analysis and sensitivity analysis. The design space is more or less distinctly divided into voids and structural elements depending on which relaxation method is applied. A broad range of design problems were solved following this approach, e.g. maximizing the structural stiffness for given mass, minimizing the weight with displacement constraints and natural frequency tuning. The numerical efficiency and the quality of the optimization results were improved applying geometrically adaptive techniques (Maute and Ramm 1995a, 1996) and including boundary variation techniques, i.e. shape optimization (Olhoff *et al.* 1991; Papalambros and Chirehdast 1993; Maute and Ramm 1995b). So far, mainly a geometrically and materially linear structural response is assumed. In order to generate a reliable design by structural optimization the nonlinear structural response, e.g. buckling or plasticity, must be considered.

Material topology optimization including geometrical nonlinearities is addressed by Neves *et al.* (1995) and by Maute (1998). The critical buckling load is maximized. The stability problem is reduced to a linearized eigenvalue problem. Truss design for nonlinear material is reported by Taylor and Lógó (1993) and Taylor (1993). The load factor is maximized limiting the maximum energy in the truss structure. The nonlinear behaviour of the material is directly considered in the formulation of the optimization problem. Material topology optimization including material nonlinearities is considered by Yuge and Kikuchi (1995). The structural stiffness of frame structures, i.e. the external work done by the applied forces, is optimized. The algorithm is based on linear Timoshenko beam theory and an elastoplastic material model with linear work-hardening. A monotonous increase of the strains is assumed. Softening and unloading are not considered. Mayer *et al.* (1996) optimize the topology of shell structures under dynamic load conditions based on an elastoplastic material model with isotropic strain hardening. The structural response is determined by a dynamic analysis, the sensitivities are approximated for quasi static conditions. In

the present paper an extended approach is presented in order to optimize the conceptual design for elastoplastic structural response. The von Mises material model with linear isotropic work-hardening/softening for small strains and plane stress conditions is applied. The derivation of a consistent sensitivity analysis is discussed in detail. The techniques and the advantages of a geometrically adaptive procedure are outlined. The implementation of the method in an overall numerical optimization procedure is presented. The proposed method is verified with numerical examples.

2 Optimization problem

In the present study the objective of the design problem is to maximize the ductility of the structure for a given range of prescribed displacements $\hat{\mathbf{u}}$. The ductility is defined by the integral of the strain energy over the range $\hat{\mathbf{u}}$. The mass $\hat{m}$ in the design space Ω is prescribed,

$$\text{minimize } f = -\int_{\Omega}\int_{\hat{\varepsilon}} \boldsymbol{\sigma}^T \,\mathrm{d}\boldsymbol{\varepsilon}\,\mathrm{d}\Omega\,, \tag{2}$$

with

$$h = \int_{\Omega} \rho\,\mathrm{d}\Omega - \hat{m} = 0\,, \tag{3}$$

where $\hat{\boldsymbol{\varepsilon}}$ are the total strains according to the prescribed displacement $\hat{\mathbf{u}}$. Additionally the mechanical equilibrium conditions must be satisfied, which are given e.g. by the principle of virtual work in its weak form

$$\int_{\Omega} \delta\boldsymbol{\varepsilon}^T \boldsymbol{\sigma}\Omega - \lambda \int_{\Gamma} \delta\mathbf{u}^T \hat{\mathbf{t}}\,\mathrm{d}\Gamma = 0\,, \tag{4}$$

where $\boldsymbol{\sigma}$ denotes the stresses, $\boldsymbol{\varepsilon}$ the strains and $\mathbf{u}$ the displacements; λ is the load factor and $\hat{\mathbf{t}}$ are the prescribed traction forces on the surface Γ. In this study body forces are neglected without loss of generality. The material distribution in the design space Ω is described by the density of the finite elements which are design variables,

$$\overline{\chi}_i = \frac{\rho_i}{\rho_0}\,, \tag{5}$$

where ρ_0 denotes the density of the homogeneous material. According to the SIMP approach the relation between material properties and the density are defined as follows:

$$\mathbf{D} = b_1(\rho_i)\mathbf{D}_0\,, \quad E^h = b_2(\rho_i)E_0^h\,, \quad \sigma_y = b_3(\rho_i)\sigma_{y_0}\,, \tag{6}$$

where $\mathbf{D}$ denotes the elastic material tensor, E^h the plastic hardening modulus, and σ_y the yield stress. The index "$_0$" marks the properties of the homogeneous material. The functions b_1, b_2, b_3 must be chosen such that the optimized design space is clearly subdivided into void and bulk material. Since in linear elasticity a β-powered material approach leads to definite results for maximum stiffness problems, b_1, b_2, b_3 are chosen analogously in the present study,

$$b_j = \left(\frac{\rho_i}{\rho_0}\right)^{\beta_j}\,, \quad j = 1,2,3\,. \tag{7}$$

The topology optimization based on an elastoplastic material model is a path-dependent problem. Instead of an engineering material approach a physically oriented approach is imaginable as well. In the case of an elastic material behaviour the material properties can be determined by a homogenization method a priori. In the case of elastoplastic material behaviour this is not possible, since the problem is path-dependent. It would be excessively costly to determine the material properties by homogenization during the nonlinear structural and sensitivity analysis (Suquet 1987; Yuge and Kikuchi 1995). Therefore, Mayer *et al.* (1996) derive only the elastic material properties by homogenization of a unit cell with a square hole and approximate the plastic properties, i.e. hardening modulus and yield stress, as functions of the density. This approach is similar to the one presented above.

The Kuhn-Tucker conditions define the optimum material distribution of the discretized optimization problem. Equations (2) and (3) yield

$$-\frac{\partial}{\partial\rho_i}\int_{\Omega_i}\int_{\hat{\varepsilon}} \boldsymbol{\sigma}^T \,\mathrm{d}\boldsymbol{\varepsilon}\,\mathrm{d}\Omega + \eta\Omega_i = 0, \tag{8}$$

$$\sum \rho_i\Omega_i - \hat{m} = 0\,, \tag{9}$$

where η is the Lagrangian multiplier and Ω_i the volume of the related finite element. In (8) $\boldsymbol{\sigma}$ and $\boldsymbol{\varepsilon}$ are assumed to be statically and kinematically admissible; i.e. the mechanical equilibrium conditions are satisfied.

The iterative algorithm to determine the optimum material distribution is split up into four parts: (i) calculate path-dependent structural response by a displacement controlled Newton-Raphson algorithm for a given design ρ_i, (ii) determine the path-dependent sensitivities of the structural response with respect to the design variables ρ_i, (iii) generate a new design by an optimality criteria method, and (iv) adapt the finite element mesh due to the material distribution obtained.

3 Nonlinear material behaviour

The material nonlinear behaviour is described by the von Mises yield criterion. The yield function $\Phi(\mathbf{S},\kappa)$ includes the deviatoric stresses $\mathbf{S}$ and the yield stress with isotropic hardening/softening as a function of the internal hardening/softening variable κ,

$$\Phi(\mathbf{S},\kappa) = |\mathbf{S}| - \sqrt{\frac{2}{3}}\sigma_\kappa \quad \text{with} \quad \mathbf{S} = \mathbf{P}\boldsymbol{\sigma}\,, \tag{10}$$

$$\sigma_\kappa = \sigma_y + E^h\kappa \quad \text{with} \quad \kappa = \sqrt{\frac{2}{3}}\gamma\,, \tag{11}$$

$\mathbf{P}$ is the projection matrix and γ the plastic multiplier. Assuming small strains, the strain increments can be partitioned into an elastic and a plastic part. Furthermore an associative flow rule is adopted,

$$\mathrm{d}\boldsymbol{\varepsilon} = \mathrm{d}\boldsymbol{\varepsilon}^{\mathrm{el}} + \mathrm{d}\boldsymbol{\varepsilon}^{\mathrm{pl}} \quad \text{with} \quad \mathrm{d}\boldsymbol{\varepsilon}^{\mathrm{el}} = \mathbf{D}^{-1}\,\mathrm{d}\boldsymbol{\sigma}\,, \tag{12}$$

$$\mathrm{d}\boldsymbol{\varepsilon}^{\mathrm{pl}} = \mathrm{d}\gamma\left|\frac{\partial\Phi}{\partial\boldsymbol{\sigma}}\right| \quad \text{with} \quad \left|\frac{\partial\Phi}{\partial\boldsymbol{\sigma}}\right| = \frac{\mathbf{S}}{|\mathbf{S}|}. \tag{13}$$

In (13) the gradient $\partial\Phi/\partial\boldsymbol{\sigma}$ is evaluated at the end of the time step for a fully implicit Euler backward algorithm. The stresses $\mathbf{S}$ must satisfy the yield function $\Phi(\mathbf{S},\kappa)$. For the Newton-Raphson method the elastoplastic compliance tensor must be derived by a consistent linearization by a consistent linearization considering the plane stress conditions (Ramm and Matzenmiller 1988),

$$\mathbf{H} = \mathbf{D}^{-1} + \mathrm{d}\gamma\frac{\partial^2\Phi}{\partial\boldsymbol{\sigma}^2}\,, \quad E_{2d}^h = \frac{E^h}{1 - 2/3E^h\,\mathrm{d}\gamma}\,,$$

and

$$\mathrm{d}\boldsymbol{\sigma} = \left(\mathbf{H}^{-1} - \frac{\mathbf{H}^{-1} \frac{\partial \Phi}{\partial \boldsymbol{\sigma}} \frac{\partial \Phi}{\partial \boldsymbol{\sigma}}^T \mathbf{H}^{-1}}{\frac{2}{3} E_{2d}^h + \frac{\partial \Phi}{\partial \boldsymbol{\sigma}}^T \mathbf{H}^{-1} \frac{\partial \Phi}{\partial \boldsymbol{\sigma}}} \right) \mathrm{d}\boldsymbol{\varepsilon} = \mathbf{D}^{\mathrm{ep}} \, \mathrm{d}\boldsymbol{\varepsilon} \,. \quad (14)$$

4 Sensitivity analysis

The sensitivity of the integral of the strain energy over the range $\hat{\boldsymbol{\varepsilon}}$ is required in order to solve the optimization problem by a gradient based optimality criteria method,

$$\frac{\partial f}{\partial \rho_i} = -\frac{\partial}{\partial \rho_i} \int_{\Omega_i} \int_{\hat{\boldsymbol{\varepsilon}}} \boldsymbol{\sigma}^T \, \mathrm{d}\boldsymbol{\varepsilon} \, \mathrm{d}\Omega =$$

$$-\frac{\partial}{\partial \rho_i} \int_{\Omega_i} \int_{\hat{\boldsymbol{\varepsilon}}} \int_{\boldsymbol{\sigma}} \mathrm{d}\boldsymbol{\sigma}^T \, \mathrm{d}\boldsymbol{\varepsilon} \, \mathrm{d}\Omega \,. \quad (15)$$

If the shape is not varied, the variation of the principle of virtual work in incremental form with respect to the design variable ρ_i yields

$$\int_{\Omega_i} \frac{\partial \left(d\boldsymbol{\sigma}^T \right)}{\partial \rho_i} \delta\boldsymbol{\varepsilon} \, \mathrm{d}\Omega - \int_{\Gamma} \frac{\partial \left[(d\lambda \hat{\mathbf{t}})^T \right]}{\partial \rho_i} \delta\mathbf{u} \, \mathrm{d}\Gamma = 0 \,. \quad (16)$$

The derivative of (14)

$$\frac{\partial d\boldsymbol{\sigma}}{\partial \rho_i} = \frac{\partial \left(\mathbf{D}^{\mathrm{ep}} \, \mathrm{d}\boldsymbol{\varepsilon} \right)}{\partial \rho_i} = \frac{\partial \mathbf{D}^{\mathrm{ep}}}{\partial \rho_i} \mathrm{d}\boldsymbol{\varepsilon} + \mathbf{D}^{\mathrm{ep}} \frac{\partial d\boldsymbol{\varepsilon}}{\partial \rho_i} \,, \quad (17)$$

and the variation of the principle of virtual work (16) lead to

$$\int_{\Omega_i} \int_{\hat{\boldsymbol{\varepsilon}}} \int_{\boldsymbol{\sigma}} \left(\mathrm{d}\boldsymbol{\varepsilon}^T \frac{\partial \mathbf{D}^{\mathrm{ep}}}{\partial \rho_i} + \frac{\partial \, \mathrm{d}\boldsymbol{\varepsilon}^T}{\partial \rho_i} \mathbf{D}^{\mathrm{ep}} \right) \mathrm{d}\boldsymbol{\varepsilon} \, \mathrm{d}\Omega =$$

$$\int_{\Gamma} \int_{\hat{\lambda}} \int_{\hat{\mathbf{u}}} \frac{\partial [(\, \mathrm{d}\lambda \hat{\mathbf{t}})^T]}{\partial \rho_i} \mathrm{d}\mathbf{u} \, \mathrm{d}\Gamma \,. \quad (18)$$

In (18) the variation of the strains is identified by $\delta\boldsymbol{\varepsilon} = d\boldsymbol{\varepsilon}$ and the variation of the displacements by $\delta\mathbf{u} = d\mathbf{u}$, respectively. The load factor $\hat{\lambda}$ corresponds to the prescribed displacements $\hat{\mathbf{u}}$ and strains $\hat{\boldsymbol{\varepsilon}}$. If the load $\hat{\mathbf{t}}$ does not depend on the design, the sensitivity of the ductility yields with (16), (17) and (18)

$$\frac{\partial f}{\partial \rho_i} =$$

$$\int_{\Omega} \int_{\hat{\boldsymbol{\varepsilon}}} \int_{\boldsymbol{\varepsilon}} \mathrm{d}\boldsymbol{\varepsilon}^T \frac{\partial \mathbf{D}^{\mathrm{ep}}}{\partial \rho_i} \mathrm{d}\boldsymbol{\varepsilon} \, \mathrm{d}\Omega - 2 \int_{\Gamma} \int_{\hat{\lambda}} \int_{\hat{\mathbf{u}}} \frac{\partial d\lambda}{\partial \rho_i} \hat{\mathbf{t}}^T \, \mathrm{d}\mathbf{u} \, \mathrm{d}\Gamma \,. \quad (19)$$

It should be taken into account that there is a difference between the sensitivities based on a displacement-controlled algorithm and those based on a load-controlled algorithm. In the case of a load-controlled algorithm the derivative of the incremental load factor $d\lambda$ is equal to zero. Displacement-controlled algorithms are more suitable for elastoplastic problems. In this case the sensitivity of the load factor $\partial d\lambda / \partial \rho_i$ is determined such that the sensitivity of the displacement $\hat{u}_j$, which is controlled during the path following procedure, is equal to zero,

$$\frac{\partial d\hat{u}_j}{\partial \rho_i} = 0 \,. \quad (20)$$

The evaluation of $\partial d\hat{u}_j / \partial \rho_i$ may be very costly in the case of topology optimization due to the large number of design variables. If $\hat{\mathbf{t}}^T d\mathbf{u} = \hat{t}_j \hat{u}_j$ is constant, i.e. only the displacement controlled point is subject to the load $\hat{t}_j$, $\partial \, \mathrm{d}\lambda / \partial \rho_i$ can be reduced to

$$\frac{\partial d\lambda}{\partial \rho_i} = \int_{\Omega} \mathrm{d}\boldsymbol{\varepsilon}^T \frac{\partial \mathbf{D}^{\mathrm{ep}}}{\partial \rho_i} \mathrm{d}\boldsymbol{\varepsilon} \, \mathrm{d}\Omega / \hat{\mathbf{t}}^T \, \mathrm{d}\mathbf{u} \,. \quad (21)$$

Equation (21) introduced into (19) yields the sensitivity of the ductility

$$\frac{\partial f}{\partial \rho_i} = -\int_{\Omega_i} \int_{\hat{\boldsymbol{\varepsilon}}} \int_{\boldsymbol{\varepsilon}} \mathrm{d}\boldsymbol{\varepsilon}^T \frac{\partial \mathbf{D}^{\mathrm{ep}}}{\partial \rho_i} \mathrm{d}\boldsymbol{\varepsilon} \, \mathrm{d}\Omega \,. \quad (22)$$

The sensitivity of the consistent elastoplastic tangent moduli $\partial \mathbf{D}^{\mathrm{ep}} / \partial \rho_i$ can be split up with respect to the elastic material tensor $\mathbf{D}$, the plastic hardening modulus E^h and the yield stress σ_y into three parts

$$\frac{\partial \mathbf{D}^{\mathrm{ep}}}{\partial \rho_i} = \frac{\partial \mathbf{D}^{\mathrm{ep}}(\mathbf{D})}{\partial \rho_i} + \frac{\partial \mathbf{D}^{\mathrm{ep}}(E^h)}{\partial \rho_i} + \frac{\partial \mathbf{D}^{\mathrm{ep}}(\sigma_y)}{\partial \rho_i} \,. \quad (23)$$

The derivatives of $\mathbf{D}$, E^h, σ_y with respect to ρ_i are

$$\frac{\partial \mathbf{D}}{\partial \rho_i} = \frac{\beta_1}{\rho_0} \rho_i^{\beta_1 - 1} \mathbf{D}_0 = \frac{\beta_1}{\rho_0} \mathbf{D} \,, \quad (24)$$

$$\frac{\partial E^h}{\partial \rho_i} = \frac{\beta_2}{\rho_0} \rho_i^{\beta_2 - 1} E_0^h = \frac{\beta_2}{\rho_0} E^h \,, \quad (25)$$

$$\frac{\partial \sigma_y}{\partial \rho_i} = \frac{\beta_3}{\rho_0} \rho_i^{\beta_3 - 1} \sigma_{y0} = \frac{\beta_3}{\rho_0} \sigma_y \,. \quad (26)$$

Subsequently it is assumed that the derivatives of the consistent elastoplastic material tensor $\mathbf{D}^{\mathrm{ep}}$ due to the change of the stress state caused by a design change in the actual increment can be neglected,

$$\frac{\partial \mathbf{D}^{\mathrm{ep}}}{\partial \boldsymbol{\sigma}} \frac{\partial \boldsymbol{\sigma}}{\partial \rho_i} = 0 \,. \quad (27)$$

Thus, the derivatives of the normal on the yield surface and the derivative of the plastic multiplier vanish,

$$\frac{\partial}{\partial \rho_i} \left(\frac{\partial \Phi}{\partial \boldsymbol{\sigma}} \right) = 0 \,, \quad \frac{\partial \, \mathrm{d}\gamma}{\partial \rho_i} = 0 \,. \quad (28)$$

This assumption is permissible for the present material model with linear work-hardening and is verified by numerical examples. In general, the derivative in (27) is not negligible. The sensitivities of the structural response, i.e. $\mathbf{u}$, $\boldsymbol{\sigma}$, $\boldsymbol{\varepsilon}$, must be determined iteratively (Lee and Arora 1995).

The first part of the gradient of the elastoplastic tangent modulus $\mathbf{D}^{\mathrm{ep}}$ is given by

$$\frac{\partial \mathbf{D}^{\mathrm{ep}}(\mathbf{D})}{\partial \rho_i} = \frac{\partial \mathbf{H}^{-1}}{\rho_i} - \omega \left(\frac{\partial \mathbf{H}^{-1}}{\rho_i} \frac{\partial \Phi}{\partial \boldsymbol{\sigma}} \frac{\partial \Phi}{\partial \boldsymbol{\sigma}}^T \mathbf{H}^{-1} \right) -$$

$$\omega \left(\mathbf{H}^{-1} \frac{\partial \Phi}{\partial \boldsymbol{\sigma}} \frac{\partial \Phi}{\partial \boldsymbol{\sigma}}^T \frac{\partial \mathbf{H}^{-1}}{\rho_i} \right) -$$

$$\frac{\partial \omega(\mathbf{D})}{\rho_i} \left(\mathbf{H}^{-1} \frac{\partial \Phi}{\partial \boldsymbol{\sigma}} \frac{\partial \Phi}{\partial \boldsymbol{\sigma}}^T \mathbf{H}^{-1} \right) \,, \quad (29)$$

with

$$\omega = \left(\frac{2}{3} E_{2d}^h + \frac{\partial \Phi}{\partial \boldsymbol{\sigma}}^T \mathbf{H}^{-1} \frac{\partial \Phi}{\partial \boldsymbol{\sigma}} \right)^{-1} \,,$$

and

$$\frac{\partial \omega(\mathbf{D})}{\rho_i} = -\omega^2 \left(\frac{\partial \Phi}{\partial \boldsymbol{\sigma}}^T \frac{\partial \mathbf{H}^{-1}}{\partial \rho_i} \frac{\partial \Phi}{\partial \boldsymbol{\sigma}} \right) \,. \quad (30)$$

The variation of (14) with respect to the design variable ρ_i leads to

$$\frac{\partial \mathbf{H}^{-1}}{\partial \rho_i} = -\mathbf{H}^{-1}\frac{\partial \mathbf{H}}{\partial \rho_i}\mathbf{H}^{-1} = \mathbf{H}^{-1}\mathbf{D}^{-1}\frac{\partial \mathbf{D}}{\partial \rho_i}\mathbf{D}^{-1}\mathbf{H}^{-1}. \quad (31)$$

Substituting (24) into (31)

$$\frac{\partial \mathbf{H}^{-1}}{\partial \rho_i} = \frac{\beta^1}{\rho_i}\mathbf{H}^{-1}\mathbf{D}^{-1}\mathbf{H}^{-1} = \frac{\beta^1}{\rho_i}\tilde{\mathbf{H}}^{-1}, \quad (32)$$

the first part of the sensitivity of $\mathbf{D}^{\mathrm{ep}}$ is equal to

$$\frac{\partial \mathbf{D}^{\mathrm{ep}}(\mathbf{D})}{\partial \rho_i} = \frac{\beta_1}{\rho_i}\left\{\tilde{\mathbf{H}}^{-1} - \omega\left(\tilde{\mathbf{H}}^{-1}\frac{\partial \Phi}{\partial \boldsymbol{\sigma}}\frac{\partial \Phi}{\partial \boldsymbol{\sigma}}^T\mathbf{H}^{-1}\right) - \omega\left(\mathbf{H}^{-1}\frac{\partial \Phi}{\partial \boldsymbol{\sigma}}\frac{\partial \Phi}{\partial \boldsymbol{\sigma}}^T\tilde{\mathbf{H}}^{-1}\right) + \omega^2\left(\frac{\partial \Phi}{\partial \boldsymbol{\sigma}}^T\tilde{\mathbf{H}}^{-1}\frac{\partial \Phi}{\partial \boldsymbol{\sigma}}\right)\left(\mathbf{H}^{-1}\frac{\partial \Phi}{\partial \boldsymbol{\sigma}}\frac{\partial \Phi}{\partial \boldsymbol{\sigma}}^T\tilde{\mathbf{H}}^{-1}\right)\right\}, \quad (33)$$

$$\frac{\partial \mathbf{D}^{\mathrm{ep}}(\mathbf{D})}{\partial \rho_i} = \frac{\beta_1}{\rho_i}\frac{\partial \tilde{\mathbf{D}}^{\mathrm{ep}}(\mathbf{D})}{\partial \rho_i}. \quad (34)$$

Analogously the second part of the gradient of the elastoplastic tangent moduli $\mathbf{D}^{\mathrm{ep}}$ is derived,

$$\frac{\partial \mathbf{D}^{\mathrm{ep}}(E^h)}{\partial \rho_i} = \omega^2\left(\mathbf{H}^{-1}\frac{\partial \Phi}{\partial \boldsymbol{\sigma}}\frac{\partial \Phi}{\partial \boldsymbol{\sigma}}^T\mathbf{H}^{-1}\right)\frac{2}{3}\frac{\partial E^h_{2d}}{\partial \rho_i} = \frac{2}{3}\frac{\beta_2}{\rho_i}\frac{E^h}{(1-2/3E^h\,\mathrm{d}\gamma)^2}\omega^2\left(\mathbf{H}^{-1}\frac{\partial \Phi}{\partial \boldsymbol{\sigma}}\frac{\partial \Phi}{\partial \boldsymbol{\sigma}}^T\mathbf{H}^{-1}\right), \quad (35)$$

$$\frac{\partial \mathbf{D}^{\mathrm{ep}}(E^h)}{\partial \rho_i} = \frac{\beta_2}{\rho_i}\frac{\partial \tilde{\mathbf{D}}^{\mathrm{ep}}(E^h)}{\partial \rho_i}. \quad (36)$$

The elastoplastic tangent modulus for the von Mises yield function does not depend on the yield stress,

$$\frac{\partial \mathbf{D}^{\mathrm{ep}}(\sigma_y)}{\partial \rho_i} = 0. \quad (37)$$

However, the derivative of the ductility with respect to the yield stress does obviously not vanish. This part of the sensitivity results from the nonsmooth material behaviour at the yield surface. The integral along the prescribed strains in (15) needs to be split up into integrals along the elastic and along the plastic deformations. The variation of the limits of integration yields the sensitivity of the ductility with respect to the yield stress. The influence of the yield stress on the ductility is illustrated by the following 1D example (Fig. 1a), which is extended to the general case.

The ductility of a truss of length $L = 1.0$ and cross-section $A = 1.0$ can be derived explicitly. The load is monotonously increased. The ductility in the elastic range ($\hat{\varepsilon} \le \sigma_y/E$) is

$$f_{\mathrm{truss}} = -\frac{1}{2}E\hat{\varepsilon}^2, \quad (38)$$

in the plastic range ($\hat{\varepsilon} > \sigma_y/E$)

$$f_{\mathrm{truss}} = -\left[\frac{1}{2}\frac{\sigma_y^2}{E} + \frac{1}{2}E_T\left(\hat{\varepsilon} - \frac{\sigma_y}{E}\right)^2 + \sigma_y\left(\hat{\varepsilon} - \frac{\sigma_y}{E}\right)\right], \quad (39)$$

where E denotes Young's modulus and E_T is the hardening modulus. The derivatives of the ductility with respect to E and E_T are consistent to (34) and (26) in (22). The variation of the limit of the integral in the plastic range, i.e. the yield stress, leads to

$$\frac{\partial f^{(\sigma_y)}_{\mathrm{truss}}}{\partial \rho_i} = -\frac{\partial \sigma_y}{\partial \rho_i}\left(\hat{\varepsilon} - \frac{\sigma_y}{E}\right)\left(1 - \frac{E_T}{E}\right). \quad (40)$$

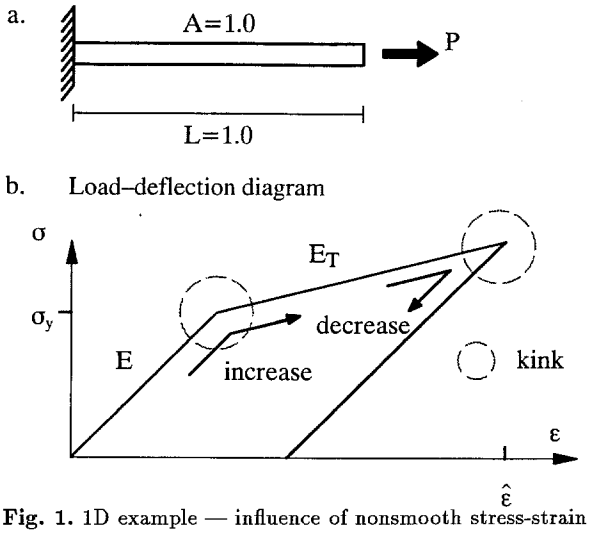

Fig. 1. 1D example — influence of nonsmooth stress-strain relation on sensitivity of ductility

This approach can be easily extended to multilinear material models. The sensitivities which result from each kink in the stress-strain relation must be added to the total sensitivities (Fig. 1b). Considering increasing and decreasing loads the sensitivity of ductility with respect to the nonsmooth stress-strain relation is extended to

$$\frac{\partial f^{(\sigma_y)}}{\partial \rho_i} = -\int_{\Omega_i}\int_{\tilde{\varepsilon}+\tilde{\tilde{\varepsilon}}}\frac{\partial \tilde{\boldsymbol{\sigma}}^T}{\partial \rho_i}\left(\mathbf{I} - \mathbf{D}^{-1}\mathbf{D}^{\mathrm{ep}}\right)\mathrm{d}\varepsilon\,\mathrm{d}\Omega - \int_{\Omega_i}\int_{\tilde{\tilde{\varepsilon}}}\frac{\partial \tilde{\tilde{\boldsymbol{\sigma}}}^T}{\partial \rho_i}\left[\mathbf{I} - (\mathbf{D}^{\mathrm{ep}})^{-1}\mathbf{D}\right]\mathrm{d}\varepsilon\,\mathrm{d}\Omega, \quad (41)$$

where $\mathbf{I}$ is the identity matrix; $\tilde{\boldsymbol{\sigma}}$ denotes the stress field when yielding begins and $\tilde{\tilde{\boldsymbol{\sigma}}}$ the stress when relieving begins, respectively; $\tilde{\varepsilon}$ marks the range of plastic deformations and $\tilde{\tilde{\varepsilon}}$ the range of relieving, respectively. The derivation of $\tilde{\tilde{\boldsymbol{\sigma}}}$ requires a complete sensitivity analysis, i.e. $\partial\boldsymbol{\sigma}/\partial\rho_i$ must be explicitly determined. For the sake of simplicity, only increasing loads are considered subsequently. The sensitivity of $\tilde{\boldsymbol{\sigma}}$ with respect to σ_y results from a variation of (10),

$$\frac{\partial \tilde{\boldsymbol{\sigma}}}{\partial \rho_i} = \sigma_y^{-1}\tilde{\boldsymbol{\sigma}}\frac{\partial \sigma_y}{\partial \rho_i}, \quad (42)$$

and with (26)

$$\frac{\partial f^{(\sigma_y)}}{\partial \rho_i} = -\int_{\Omega_i}\int_{\tilde{\varepsilon}}\frac{\beta_3}{\rho_i}\tilde{\boldsymbol{\sigma}}^T\left(\mathbf{I} - \mathbf{D}^{-1}\mathbf{D}^{\mathrm{ep}}\right)\mathrm{d}\varepsilon\,\mathrm{d}\Omega. \quad (43)$$

With (34), (36) and (43) the derivative of the ductility with respect to the density ρ_i yields

$$\frac{\partial f}{\partial \rho_i} = \frac{1}{\rho_i}\frac{\partial \tilde{f}}{\partial \rho_i}, \quad (44)$$

with

$$\frac{\partial \tilde{f}}{\partial \rho_i} = -\int_{\Omega_i}\int_{\hat{\varepsilon}}\int_{\varepsilon}\mathrm{d}\varepsilon^T\left[\beta_1\frac{\partial \tilde{\mathbf{D}}^{\mathrm{ep}}(\mathbf{D})}{\partial \rho_i} + \beta_2\frac{\partial \tilde{\mathbf{D}}^{\mathrm{ep}}(E^h)}{\partial \rho_i} + \right]\mathrm{d}\varepsilon\,\mathrm{d}\Omega - \int_{\Omega_i}\int_{\hat{\varepsilon}}\beta_3\tilde{\boldsymbol{\sigma}}^T\left(\mathbf{I} - \mathbf{D}^{-1}\mathbf{D}^{\mathrm{ep}}\right)\mathrm{d}\varepsilon\,\mathrm{d}\Omega. \quad (45)$$

Mayer *et al.* (1996) applied a considerably simplified approach. Instead of the sensitivities of the consistent material tensor, only the sensitivities of the elastic tangent in the elastic range and the elastoplastic tangent in the plastic range are determined. The sensitivities of the energy due to a variation of the yield stress are neglected.

5 Implementation of structural and sensitivity analysis

The numerical procedure to determine the structural response, the ductility and the sensitivities of the ductility is shown in Fig. 2.

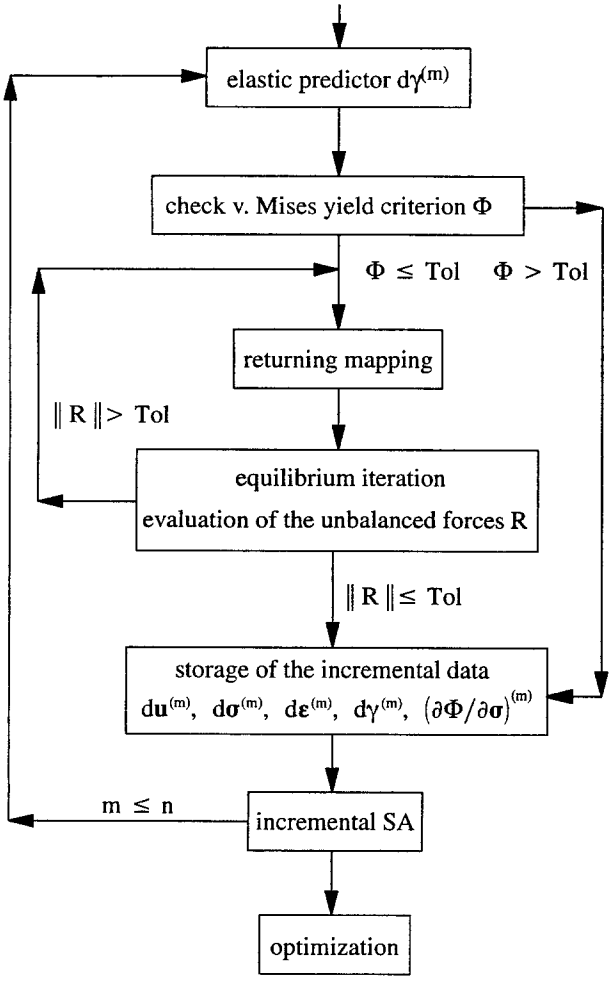

Fig. 2. Numerical implementation of elastoplastic structural analysis and sensitivity analysis

The incremental procedure is based on the Newton-Raphson-method. The stress increments $\Delta\sigma^{(m)}$ and strain increments $\Delta\varepsilon^{(m)}$ are determined by a fully implicit Euler backward algorithm. The index "(m)" marks the load increment and "n" is the total number of increments. The increase of the ductility $\Delta f^{(m)}$ is evaluated for each load increment by

$$f = -\sum_{m=1}^{n} \Delta f^{(m)},$$

with

$$\Delta f^{(m)} = \frac{1}{2}\Delta\varepsilon^{(m)}\Delta\sigma^{(m)} + \Delta\varepsilon^{(m)}\Delta\sigma^{(m-1)}. \tag{46}$$

Thus, the ductility is determined with a mean material tensor $\tilde{\mathbf{D}}^{\mathrm{ep}(m)}$ (Fig. 3).

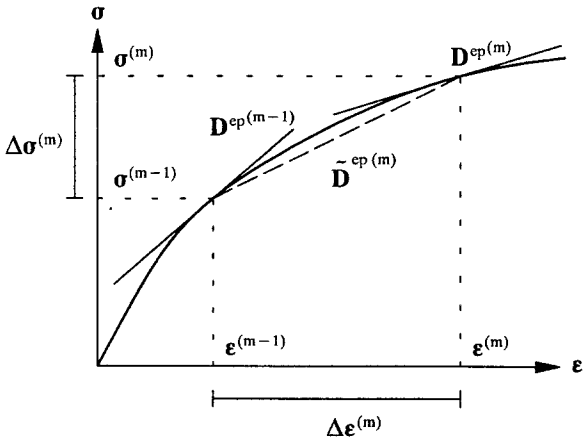

Fig. 3. Tangential and mean material tensor

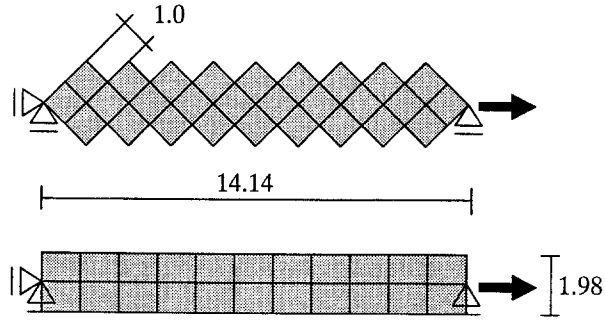

Material data:

Young's modulus:	$E = 180000\ \mathrm{kN/m^2}$
Plastic hard. modulus:	$E^h = 0.1\ \mathrm{kN/m^2}$
Yield stress:	$\sigma_y = 36.0\ \mathrm{kN/m^2}$
Poisson ratio:	$\nu = 0.0$
Volume:	$V = 28.0\ \mathrm{m^3}$

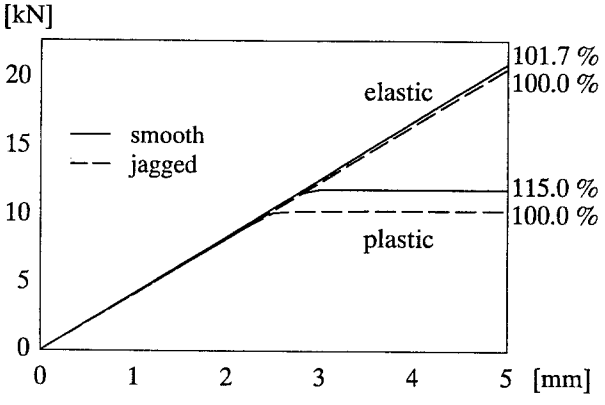

Fig. 4. Smooth and jagged tension bar

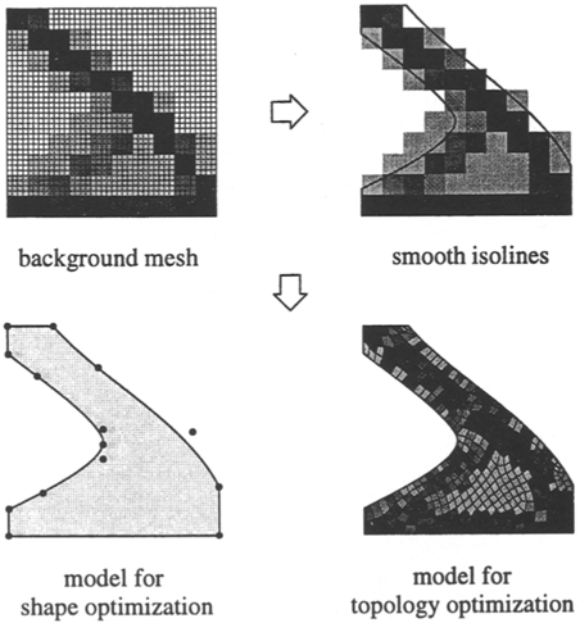

Fig. 5. Adaptation of design model

Since the material tensor can be determined only at the end of each load increment, $\Delta f^{(m)}$ is written in terms of $\mathbf{D}^{\mathrm{ep}(m)}$,

$$\Delta f^{(m)} = \frac{1}{2}\Delta\varepsilon^{*(m)^T}\mathbf{D}^{\mathrm{ep}(m)}\Delta\varepsilon^{(m)} + \Delta\varepsilon^{(m)}\Delta\sigma^{(m-1)},$$

with

$$\Delta\varepsilon^{*(m)} = (\mathbf{D}^{\mathrm{ep}})^{-1^{(m)}}\Delta\sigma^{(m)}. \tag{47}$$

Equations (46) and (47) are equivalent with respect to the ductility, but not with respect to the derivative of the ductility. According to (44) and (45) the derivatives must be determined analogously to (47). The derivative of the ductility consists of two parts,

$$\frac{\partial\tilde{f}}{\partial\rho_i} = -\frac{\partial\tilde{f}_1}{\partial\rho_i} - \frac{\partial\tilde{f}_2}{\partial\rho_i}. \tag{48}$$

The first part corresponds to the first integral of (45),

$$\frac{\partial\tilde{f}_1}{\partial\rho_i} = \sum_{m=1}^{n}\frac{\partial\tilde{f}_1}{\partial\rho_i}^{(m)}, \tag{49}$$

with

$$\frac{\partial\tilde{f}_1}{\partial\rho_i}^{(m)} = \frac{1}{2}\Delta\sigma^{(m)}\mathbf{D}^{*(m)}\Delta\varepsilon^{(m)} + \Delta\sigma^{(m)}\Delta\varepsilon^{*(m)}, \tag{50}$$

$$\Delta\varepsilon^{*(m)} = \sum_{k=1}^{m-1}\mathbf{D}^{*(k)}\Delta\varepsilon^{(k)}, \tag{51}$$

$$\mathbf{D}^{*(m)} = \left\{(\mathbf{D}^{\mathrm{ep}})^{-1}\left[\beta_1\frac{\partial\tilde{\mathbf{D}}^{\mathrm{ep}}(\mathbf{D})}{\partial\rho_i} + \beta_2\frac{\partial\tilde{\mathbf{D}}^{\mathrm{ep}}(E^h)}{\partial\rho_i}\right]\right\}^{(m)}. \tag{52}$$

The second part considers the influence of the variation of the yield stress. Again, only increasing loads are considered, but the algorithm can be easily extended to the decreasing loads,

$$\frac{\partial\tilde{f}_2}{\partial\rho_i} = \sum_{m=1}^{n}\sigma_y^{*^T}\Delta\varepsilon^{(m)}. \tag{53}$$

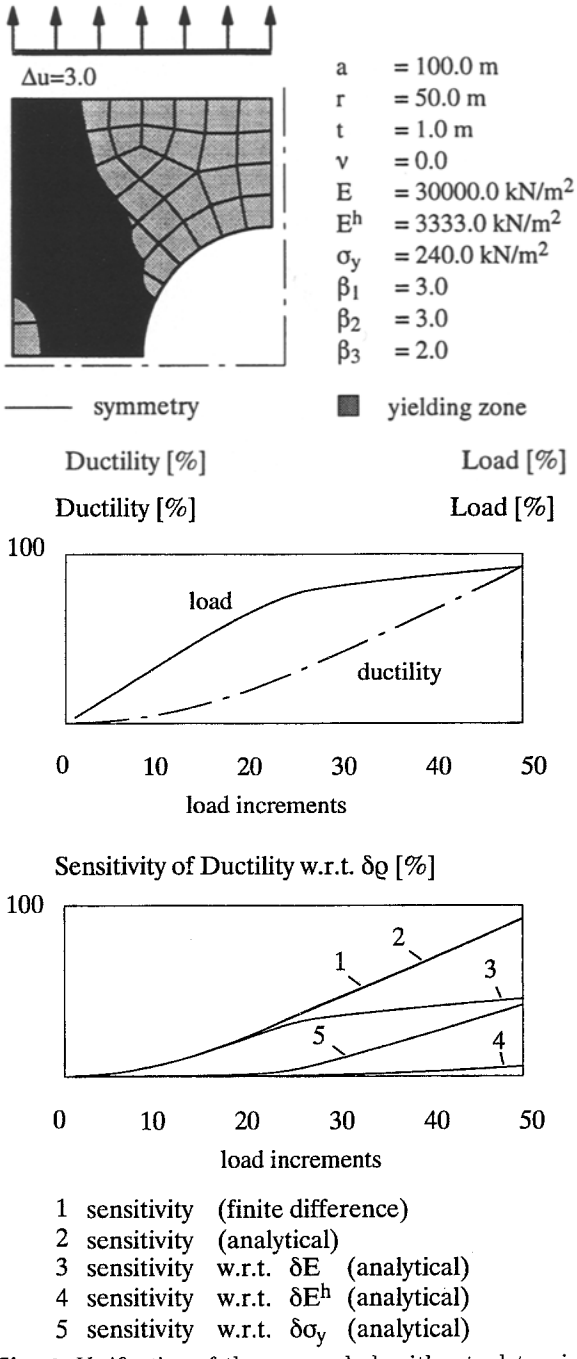

Fig. 6. Verification of the proposed algorithm to determine the sensitivity of the ductility

At the beginning of the incremental analysis σ_y^* is equal to zero. If yielding begins, i.e. the plastic multiplier $\gamma^{(m)}$ turns from zero to a positive value, σ_y^* is set to

$$\sigma_y^* = \beta_3\left(\mathbf{I} - \mathbf{D}^{-1}\mathbf{D}^{\mathrm{ep}}\right)\sigma^{(m)}. \tag{54}$$

A crucial point is that the yield stress σ_y^* and the range of plastic deformations $\tilde{\varepsilon}$ cannot exactly be determined in this projection method. However, the resulting error can be neglected in general. This was verified by several numerical examples.

The evaluation of this procedure requires the storage of $\sigma^{(m)}$, $\sigma^{(m-1)}$, $\varepsilon^{(m)}$, $\varepsilon^{(m-1)}$, $(\partial\Phi/\partial\sigma)^{(m)}$,$(\partial\Phi/\partial\sigma)^{(m-1)}$,

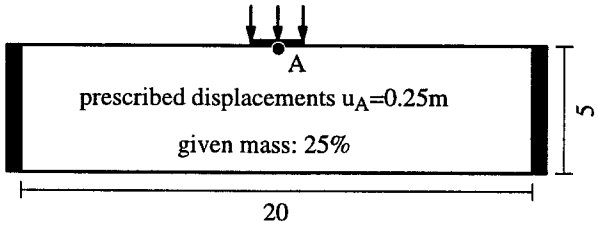

Material data:

Young's modulus	$E = 180000\ kN/m^2$
Plastic hard. modulus	$E^h = 0.1\ kN/m^2$
Yield stress	$\sigma_y = 360\ kN/m^2$
Poisson Ratio	$\nu = 0.0$
Multipliers	$\beta_1 = 3.0, \beta_2 = 3.0, \beta_3 = 2.0$

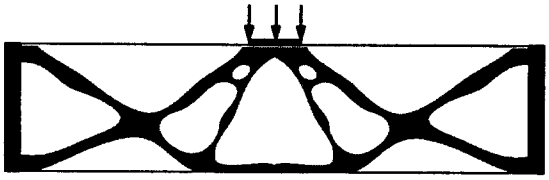

Optimization result (plastic)

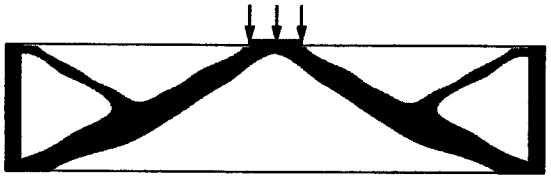

Optimization result (elastic)

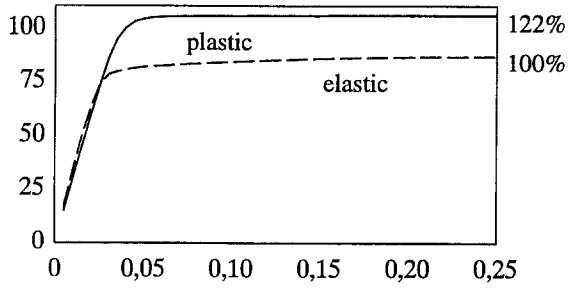

Load–deflection–diagram

Fig. 7. Example 1 — clamped beam

$\gamma^{(m)}$, $\gamma^{(m-1)}$, and $\boldsymbol{\sigma}_y^*$ for each Gaussian point.

6 Optimality criteria method

Optimality criteria methods are efficient and robust in particular for optimization problems with a large number of design variables and with only few constraints when the set of active constraints and the related Lagrange multipliers can directly be determined. Substituting (45) into (8) the Kuhn-Tucker condition equals

$$\frac{1}{\rho_i}\frac{\partial \tilde{f}}{\partial \rho_i} + \eta \Omega_i = 0\,, \tag{55}$$

and the following simple but efficient update scheme is derived:

$$\rho_i{}^{(k+1)} = \rho_i{}^{(k)} \left(-\frac{1}{\eta m_i}\frac{\partial \tilde{f}}{\partial \rho_i} \right)^{(k)\mu}\,, \tag{56}$$

where (k) denotes the current iteration in the optimization process and m_i is the mass in the design patch i. The exponent μ is introduced to control the convergence of the optimization process. If μ is too large oscillations may occur, if μ is too small the rate of convergence is low. Usually μ is chosen in the range between 0.5 and 0.8. The Lagrange multiplier η is determined from (9) such that the equality constraint for the mass is satisfied.

7 Adaptive topology optimization

The main shortcomings of conventional material topology optimization are the large number of optimization variables and nonsmooth, indefinite results. Moreover in elastoplasticity, jagged boundaries cause stress singularities which introduce artificial yielding. Truss- and bar-like structural elements are often generated by topology optimization. The structural response of a truss with jagged boundaries is compared to one with smooth boundaries (Fig. 4). Both trusses are of the same length, volume and loading conditions. The load-deflection curves are determined for a prescribed tip displacement $\hat{u}_A$=5 mm. If a linear elastic material behaviour is assumed the difference between the jagged truss and the smooth one is only 1.7 percent. However, in the case of elastoplastic material behaviour the jagged boundaries introduce artificial yielding. Without hardening the load of the jagged truss is about 15 percent less compared with the load of the smooth truss.

These problems can be overcome adapting the design model to the current material distribution during the optimization process (Maute and Ramm 1995a). The fundamental idea of the proposed algorithm is to generate isolines of the material distribution. These isolines can be used to define the outer contours of the new design model. The adaptive optimization process can be split up into three steps.

1. Solving the optimization problem for a given parametrization by material topology optimization.
2. Storing the optimization results on a background mesh and determining the parametrization in the subsequent design model.
3. Updating the design model, defining the new set of optimization variables and generating a new analysis model.

The topology optimization problem is solved for a given parametrization of the design space, i.e. the finite element mesh. After the material distribution is mapped onto the background mesh in the parameter space it can be optionally filtered, i.e. the material distribution can be lumped or smoothed. The isolines for one or more density levels are determined. For this the elemental material data of the finite elements are transferred to nodal data. The points of one isoline are determined on the boundaries of the finite elements by linear interpolation of the nodal density values. By connecting these points by polygons the isolines are obtained. In order to obtain smooth boundaries the polygons are approximated by splines. The approximation tolerance, i.e. the

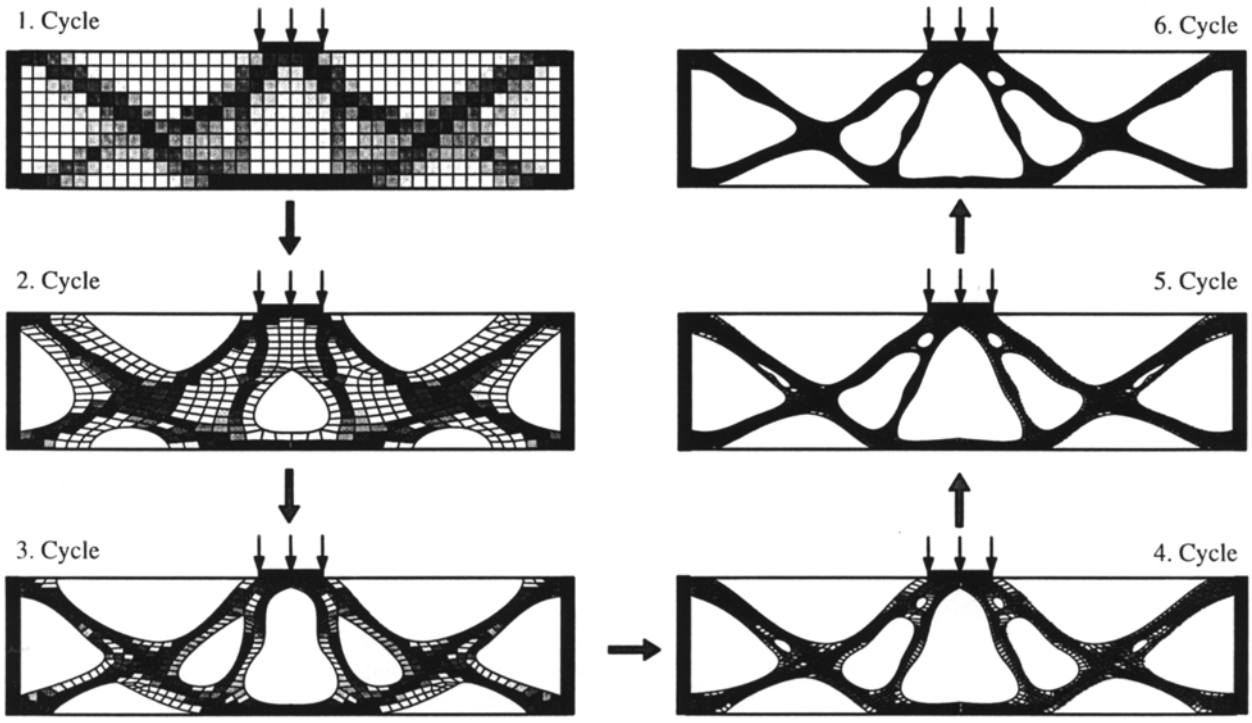

Fig. 8. Example 1 — adaptation of design model

area between the splines and the polygons can be prescribed. The approximation error can be reduced by increasing the number of splines. Since an adaptive approximation procedure is used, the segmentation by splines can be optimized. Domains with density values below a certain threshold value are considered as voids and are therefore neglected in the following optimization step. Finally, the generated structural layout is parametrized and the optimization variables are defined depending on the kind optimization applied next. For further details the reader is referred to the paper by Maute and Ramm (1995a).

This procedure is illustrated with a simple example in Fig. 5. In the parameter space a quadratic design space is given. The background mesh contains 900 square patches. The current material distribution is shown. The isolines for a density ratio of 10 percent are determined and the design models for shape and topology optimization are generated.

With this so-called adaptive topology optimization it is possible to reduce the number of optimization variables and, at the same time, to increase the quality of the optimization result.

8 Numerical examples

8.1 Verification of sensitivities

First, the proposed algorithm determining the sensitivity of the ductility is verified by an example. The structural situation and the material properties are given in Fig. 6. The optimization variable is the density of the overall structure. In the upper diagram the load and the structural ductility over the range of the prescribed displacement are presented. The dark area in the structure represents the yielding zone. The lower diagram shows that the analytical sensitivity determined by the proposed algorithm and the numerical sensitivity determined by a finite difference scheme are exactly the same. The remaining curves represent the different parts of the overall sensitivity.

8.2 Examples

The proposed algorithm is verified by three examples for plane stress conditions. The objective of all design problems is to maximize the structural ductility for a range of prescribed displacements $\hat{u}_A$. The degrees of freedom of the loaded nodes are coupled. The material data are given in the related figures. Due to the symmetry of the problems only on half of the structures are analysed. At the beginning of the optimization process the entire design space is equally filled with porous material. The optimum material distribution for a coarse mesh is roughly determined applying the OC method according to (56). Based on this material distribution an adapted design model with a finer mesh is generated neglecting void domains. The optimized layout is determined assuming an elastic structural behaviour in order to show the differences between the optima based on an elastic and an elastoplastic material behaviour. In the elastic case the optimal topology is obtained based on a linear material model. Subsequently the ductility of the optimized structure is determined for elastoplastic material behaviour. The following figures show the structural situation, the optimal topologies based on an elastic material behaviour and on an elastoplastic material behaviour, respectively, and the related load-deflection diagrams.

8.2.1 Example 1. The structural situation of the first example is shown in Fig. 7. The beam is clamped on both sides and subjected to a vertical load in the centre of the upper edge. The optimized material distributions for the different

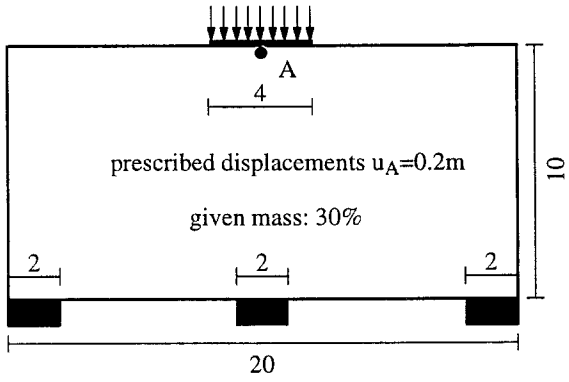

Material data:

Young's modulus	E	= 30000 kN/m^2
Plastic hard. modulus	E^h	= 0.1 kN/m^2
Yield stress	σ_y	= 240 kN/m^2
Poisson Ratio	ν	= 0.0
Multipliers	β_1	=2.5, β_2 =2.5, β_3=2.0

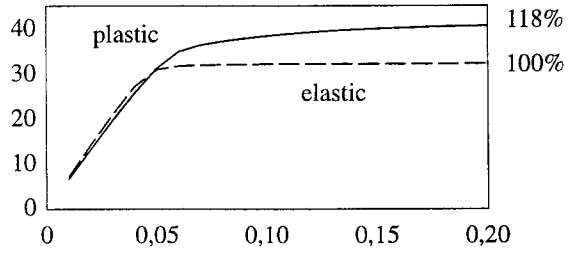

Load–deflection–diagram

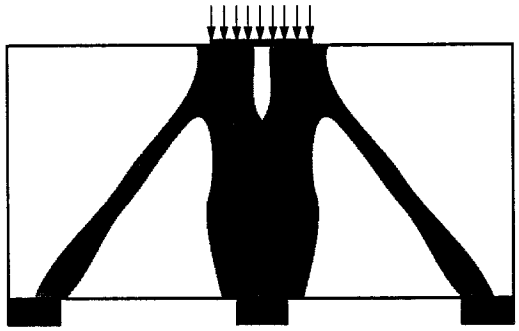

Optimization result (plastic)

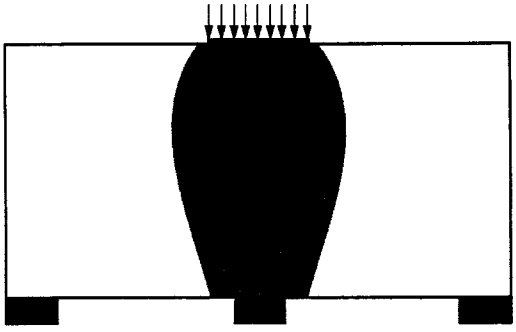

Optimization result (elastic)

Fig. 9. Example 2 — pier

discretizations of the design model during the adaptive optimization procedure are given in Fig. 8. The final result based on an elastoplastic material model is shown. The elastoplastic optimum differs considerably from the optimized topology based on an elastic material model. In the elastoplastic case the available supports are equally used, which in turn causes a different internal layout. The ductility of the elastoplastic optimum is about 22 percent larger in comparison to the elastic one. The stiffness of the elastoplastic optimum is slightly smaller in the elastic range, but yielding begins at a higher load level.

8.2.2 Example 2. In the second example it is clearly illustrated that structures optimized with respect to an elastoplastic material behaviour equally use available supports. The structural situation and the material data are given in Fig. 9. The vertical loads are distributed over a length of 4 m, the length of each support is 2 m. In this example the adaptive procedure is repeated three times until the layout converges. The elastic optimum is a straight pier. In the elastoplastic optimum the loads are carried by all three supports, which reduces the stress concentration at the supports. The objective of the elastoplastic optimum is about 18 percent higher than the elastic one. Again, the stiffness of the elastoplastic optimum is slightly smaller in the elastic range, but yielding begins at a higher load level in comparison to the elastic optimum.

8.2.3 Example 3. In the first two examples the layouts of the elastic and elastoplastic optima are quite different. In this example it is shown that even small changes of the layout may cause a large difference of the elastoplastic structural response. A bow-type beam structure is bounded by two single supports (Fig. 10). The optimized topologies based on an elastic and elastoplastic material models are similar, since all supports must be used to satisfy the global equilibrium. However, the ductility of the elastoplastic optimum is about 110 percent larger in comparison to the ductility of the elastic optimum. The length of the used support dx differs considerably. The length dx is two times bigger considering an elastoplastic material behaviour in comparison to the elastic case.

9 Discussion

A procedure optimizing the ductility for given mass by adaptive material topology optimization was presented and verified by numerical examples for plane stress conditions. The results show that is important to consider the material nonlinear structural response in the optimization process. The quality of layouts obtained by structural optimization assuming an elastic structural response is of limited value in the case of nonlinear elastoplastic material behaviour. The proposed algorithm proved to be efficient and robust for other design problems as well. Jagged boundaries which may lead

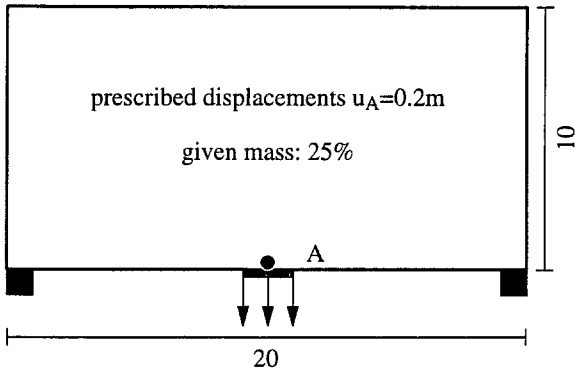

Material data:

Young's modulus	$E = 30000\ kN/m^2$
Plastic hard. modulus	$E^h = 0.1\ kN/m^2$
Yield stress	$\sigma_y = 240\ kN/m^2$
Poisson Ratio	$\nu = 0.0$
Multipliers	β_1 =2.5, β_2 =2.5, β_3=2.0

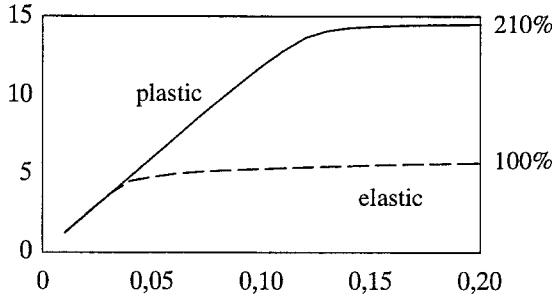

Load–deflection–diagram

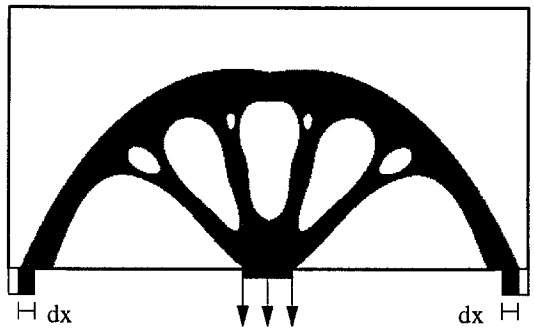

Optimization result (plastic)

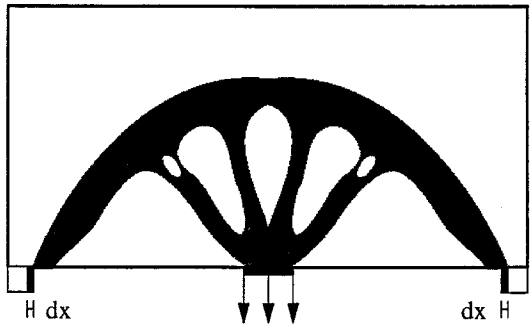

Optimization result (elastic)

Fig. 10. Example 3 — bow-type beam

to stress singularities and incorrect optimization results are avoided by an adaptive procedure. The adaptive procedure also reduces the numerical effort and provides a direct link to the shape optimization. The integration of topology and shape optimization in elastoplastic design will be investigated in further studies.

Acknowledgements

This work is part of the DFG research projects Ra 218/16–1 "Adaptive Methods in Topology Optimization" and Ra 218/11–1 "Algorithms, Adaptive methods, Elastoplasticity". The support is gratefully acknowledged. The second author would like to acknowledge the financial support provided by the Swiss foundation "Besinnung und Ordnung".

References

Bendsøe, M.P. 1995: *Optimization of structural topology, shape and material.* Berlin, Heidelberg, New York: Springer

Bendsøe, M.P.; Mota Soares, C.A. 1991: *Topology design of structures.* Dordrecht: Kluwer

Kohn, R.V.; Strang, G. 1986: Optimal design and relaxation of variational problems. *Comm. Pure Appl. Math.* **36**, 113–137, 139–182, 353–377

Lee, T.H.; Arora, J.S. 1995: A computational method for design sensitivity of elastoplastic structures. *Comp. Meth. Appl. Mech. Eng.* **122**, 27–50

Maute, K. 1998: *Topologie- und Formoptimierung von dünnwandigen Tragwerken.* Ph.D. Thesis, University of Stuttgart (to be published)

Maute, K.; Ramm, E. 1995a: Adaptive topology optimization. *Struct. Optim.* **10**, 100–112

Maute, K.; Ramm, E. 1995b: General shape optimization — an integrated model for topology and shape optimization. In: Olhoff, N.; Rozvany, G.I.N. (eds.) *Proc. WCSMO-1, First World Congress of Structural and Multidisciplinary Optimization* (held in Goslar, Germany), pp. 229–306. Oxford: Pergamon

Maute, K.; Ramm, E. 1996: Adaptive topology optimization of shell strucures. *Proc. 6-th AIAA/NASA/ISSMO Symp. on Multidisciplinary Analysis and Optimization*, pp. 1133–1141. AIAA

Mayer, R.R.; Kikuchi, N.; Scott, R.A. 1996: Application of topological optimization techniques to structural crashworthiness. *Int. J. Num. Meth. Eng.* **39**, 1383–1403

Mlejnek, H.P. 1993: Some aspects of the genesis of structures. *Struct. Optim.* **5**, 64–69

Neves, M.M.; Rodrigues, H.; Guedes, J.M. 1995: Generalized topology design of structures with buckling load criterion. *Struct. Optim.* **10**, 71–78

Olhoff, N.; Bendsøe, M.P.; Rasmussen, J. 1991: On CAD-integrated structural topology and design optimization. *Comp. Meth. Appl. Mech. Eng.* **89**, 259–279

Papalambros, P.Y.; Chirehdast, M. 1993: Integrated structural optimization systems. In: Bendsøe, M.P.; Mota Soares, C.A. (eds.) *Topology design of structures*, pp. 501–514. Dordrecht: Kluwer

Ramm., E.; Matzenmiller, A. 1988: Consistent linearization in elasto-plastic shell analysis. *Eng. Comp.* **5**, 289–299

Rozvany, G.I.N.; Bendsøe, M.P.; Kirsch, U. 1995: Layout optimization of structures. *Appl. Mech. Rev.* **48**, 41–119

Rozvany, G.I.N.; Zhou, M. 1990: Applications of the COC method in layout optimization. In: Eschenauer, H.; Mattheck, C.; Olhoff, N. (eds.) *Proc. Conf. on Engineering Optimization on Design Processes* (held in Karlsruhe), pp. 59–70. Berlin, Heidelberg, New York

Rozvany, G.I.N.; Zhou, M.; Birker, T. 1992: Generalized shape optimization without homogenization. *Struct. Optim.* **4**, 250–252

Suquet, P.M. 1987: Elements of homogenization for inelastic solid mechanics. In: Sanches-Palencia, E.; Zaoui, A. (eds.) *Homogenization techniques for composite media*, pp. 193–278. Berlin, Heidelberg, New York: Springer

Taylor, J.E.; Lógó, J. 1993: Analysis and design of elastic/softening truss structures based on a mixed-form extremum principle. In: Rozvany, G.I.N. (ed.) *Optimization of large structural systems* (Proc. NATO/DFG ASI held in Berchtesgaden, Germany, 1991), pp. 683–696. Dordrecht: Kluwer

Taylor, J.E. 1993: Truss topology design for elastic/softening materials. In: Bendsøe, M.P.; Mota Soares, C.A. (eds.) *Topology design of structures*, pp. 451–467. Dordrecht: Kluwer

Yuge, K.; Kikuchi, N. 1995: Optimization of a frame structure subjected to a plastic deformation. *Struct. Optim.* **10**, 197–208

Received Aug. 6, 1997
Revised manuscript received Dec. 13, 1997

Announcement

International Centre for Mechanical Sciences (CISM)
Programme 1998

Advanced Professional Training
Mechanics and Design of Tubular Structures
Coordinators: J. Farkas, K. Jarmai (Miskolc) June 1-5

Computational Biology
Coordinators: P. Serafini (Udine),
R. Ravi (Pittsburgh) June 10-19

Evironmental Fluid Mechanics
Coordinator: G.H. Jirka (Karlsruhe) June 22-26

Identification of Media and Structures by Inversion of Mechanical Wave Propagation
Coordinator: A. Wirgin (Marseille) July 13-17

Kinetic and Continuum Thermodynamical Approaches to Granular and Porous Media
Coordinators: K. Wilmanski (Berlin),
K. Hutter (Darmstadt) July 13-17

IUTAM Summer School
Advanced Turbulent Flow Computations
Coordinators: R. Peyret (Nice),
E. Krause (Aachen) September 7-11

Modelling of Creep and Damage Processes in Materials and Structures
Coordinators: H. Altenbach (Halle),
J. Skrzypek (Krakow) September 7-11

Fluid Structure Interactions in Acoustics
Coordinators: D. Habault (Marseille), N. Peake
(Cambridge), van der Burgh (Delft) September 14-18

Wind-Resistant Design of Structures: Codified and Advanced Methods
Coordinators: G. Augusti (Roma),
H.J. Niemann (Bochum) September 21-25

Multibody Dynamics with Unilateral Contacts
Coordinators: P. Pfeiffer,
C. Glocker (München) September 28-October 2

Modern Optical Methods in Experimental Solid Mechanics
Coordinator: K.H. Laermann (Wuppertal) October 5-9

Neural Networks in Mechanics of Structures and Materials
Coordinator: Z. Waszczyszyn (Krakow) October 19-23

Palazzo del Torso, Piazza Garibaldi 18, 33100 Udine, Italy
tel.: +39(432)294989 or 508251 - fax 501523 - e-mail: cism@cc.uniud.it - http://www.uniud.it/cism/homepage.htm